SARS-Cov-2 Delta Variant Decreases Nanobody Binding and ACE2 Blocking Effectivity

*Mert Golcuk[1], Aysima Hacisuleyman[2], Sema Zeynep Yilmaz[1], Elhan Taka[1], Ahmet Yildiz[3,4], Mert Gur[1]**

[1] Department of Mechanical Engineering, Istanbul Technical University (ITU), 34437, Istanbul, Turkey

[2] Institute of Bioengineering, Swiss Federal Institute of Technology (EPFL), 1015, Lausanne, Switzerland

[3] Physics Department, University of California, 94720, Berkeley, CA, USA

[4] Department of Molecular and Cellular Biology, University of California, 94720, Berkeley, CA, USA

* Corresponding Author; e-mail: gurme@itu.edu.tr

Keywords: Nanobody, Delta Variant, COVID-19, SARS-CoV-2, Molecular Dynamics Simulations, Steered Molecular Dynamics Simulations, Spike Glycoprotein

ABSTRACT

The Delta variant spreads more rapidly than previous variants of SARS-CoV-2. This variant comprises several mutations on the receptor-binding domain (RBD_{Delta}) of its spike (S) glycoprotein, which binds to the peptidase domain (PD) of angiotensin-converting enzyme 2 (ACE2) receptors in host cells. The RBD-PD interaction has been targeted by antibodies and nanobodies to prevent viral infection, but their effectiveness against the Delta variant remains unclear. Here, we investigated RBD_{Delta}-PD interactions in the presence and absence of nanobodies H11-H4, H11-D4, and Ty1 by performing in a total of 19 μs all-atom molecular dynamics (MD) simulations. Unbiased simulations revealed that Delta variant mutations strengthen RBD binding to ACE2 by increasing the hydrophobic interactions and salt bridge formation, but weaken interactions with H11-H4, H11-D4, and Ty1. Consequently, these nanobodies are unable to dislocate ACE2 from RBD_{Delta}. Steered MD simulations at comparable loading rates to atomic force microscopy (AFM) experiments estimated lower rupture forces of the nanobodies from RBD_{Delta} compared to ACE2. Our results suggest that existing nanobodies are less effective to inhibit RBD_{Delta}-PD interactions and a new generation of nanobodies will be needed to neutralize the Delta variant.

INTRODUCTION

Nanobodies are promising alternatives to conventional antibodies because they are smaller in their size (15 kDa),[1] have similar affinity to conventional antibodies, enter the cell more readily, and can be mass-produced at lower cost.[2, 3] The small size of the nanobodies also enables them to bind epitopes normally not accessible to conventional antibodies,[4] including conserved viral domains often masked by glycan shields.[5] Currently there are more than 180 neutralizing nanobodies targeting the SARS-CoV-2 spike (S) glycoprotein[6] and the structures of more than 30 nanobodies have been recently solved.[7] Most of these nanobodies have shown promising neutralizing activity against wild type (WT) SARS-CoV-2,[2, 3, 5, 8-16] but their effectivity against the Delta variant remains to be elucidated.

Currently, the Delta (B.1.617.2) variant is the most dominant variant with the highest number of reported cases.[17, 18] The Delta variant comprises 10 mutations on the homotrimeric S protein (Figure 1), which is the critical protein that mediates host cell entry of the virus via binding of its receptor-binding domain (RBD) to the angiotensin-converting enzyme 2 (ACE2) receptor of the host cells. Two of these mutations are located on the ACE2 binding surface of RBD (L452R and T478K), while five mutations are located on the N terminal domain (NTD) surface (T19R, G142D, E156del, F157del, and R158G), and three mutations are located in S2 (D614G, P681R, and D950N).[17, 19, 20] These mutations are positioned on the binding interfaces for a wide range of antibodies and nanobodies; thus, potentially affecting their binding strengths. Consistent with this view, recent experimental studies revealed substantial decrease in the neutralization activity of many nanobodies while only a few kept their neutralization activity.[19, 21-23] Similarly, the Delta variant exhibited higher resistance to neutralizing antibodies formed by major vaccines, including mRNA vaccines (mRNA-1273 and BNT162b2)[24, 25] and adenovirus vector vaccines (Sputnik V and ChAdOx1).[26, 27] However, the underlying mechanism of the reduced effectiveness of the nanobodies against the Delta variant is not well understood.

In our recent study, we performed extensive molecular dynamics (MD) simulations of the nanobodies H11-H4, H11-D4 and Ty1 in complex with WT, Alpha and Beta variants of the RBD of SARS-CoV-2 S protein.[28] We showed that the Delta variant mutation L452R is located at the hydrophobic core of the nanobody-RBD interface for WT SARS-CoV-2. Thus, it remains to be explored how this mutation affects the binding strength. A recent in vitro and in silico study[29] estimated that the S protein of the Alpha variant of SARS-CoV-2 binds to ACE2 stronger than that of the Delta variant. Considering that Delta became more dominant than the Alpha variant, it is also critical to investigate how these novel mutations affect the effectiveness of antibodies and nanobodies to prevent S-ACE2 interactions.

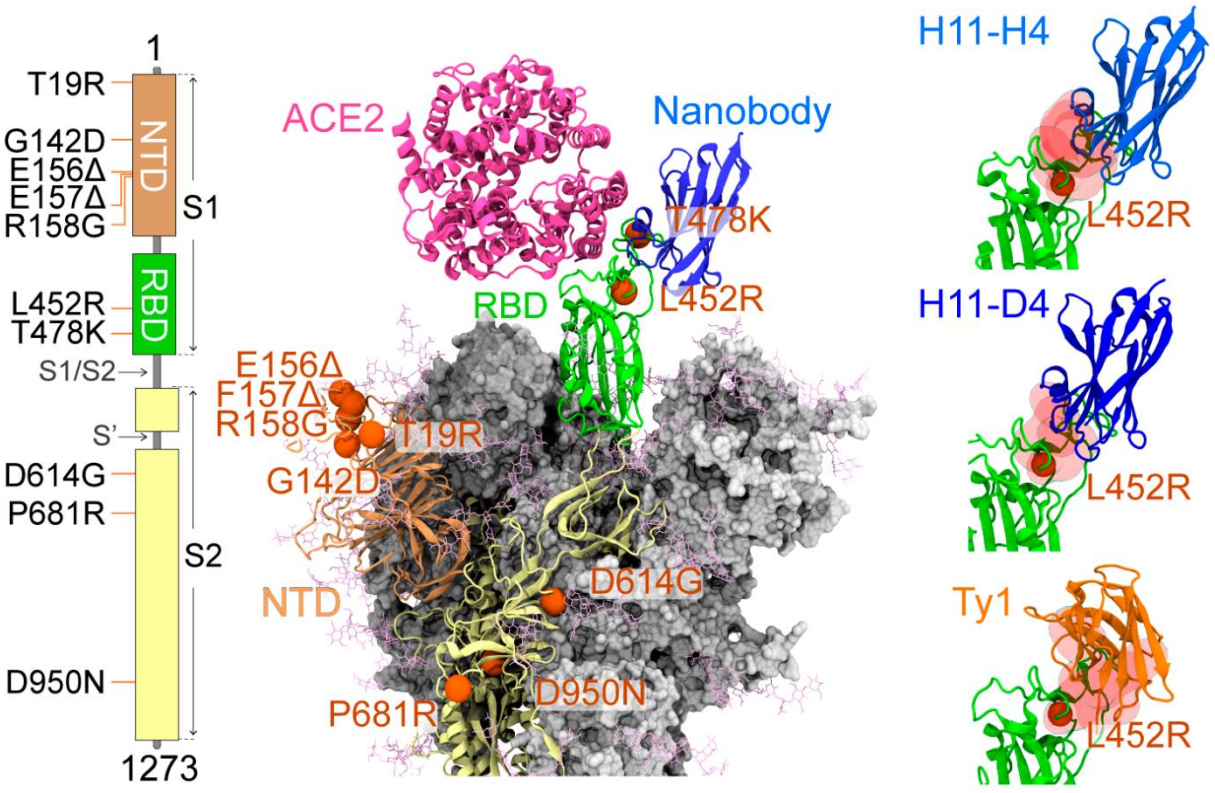

Figure 1. Locations of the mutations observed in Delta variant shown on S protein structure. Sites of the 10 mutations of the Delta variant are highlighted with orange spheres. Crystal structures of nanobodies (PDB IDs: 6ZBP,[9] 6YZ5,[9] and 6ZXN[2]) and ACE2 (PDB ID: 6M0J[30]) are docked onto RBD_{Delta}.

In order to explore the effect of Delta variant mutations on neutralizing nanobodies, we performed all-atom MD simulations of RBD_{Delta} in complex with either the peptidase domain (PD) of human ACE2 or nanobodies H11-H4, H11-D4 and Ty1. We also simulated the detachment of the nanobodies from RBD at loading rates directly comparable to high-speed atomic force microscopy (AFM) studies.[31] Our simulations totaling 19 μs in length show that the Delta variant mutations increase the binding strength of RBD_{Delta} to ACE2, while reducing the binding strength of the nanobodies to RBD_{Delta}. These nanobodies are also not able to dislocate ACE2 from RBD_{Delta} upon binding, indicating lower neutralizing activity against this variant.

METHODS

System Preparations for MD Simulations. The structure of SARS-CoV-2 S protein RBD bound with ACE2 at 2.45 Å resolution (PDB ID: 6M0J[30]) was used as a template for the MD simulations of the RBD-ACE2 complex. In order to obtain the Delta variant structure, L452R and T478K mutations were performed on the RBD using Mutator plugin of Visual Molecular Dynamics (VMD).[32] Crystal structures of nanobodies (PDB IDs: 6ZBP,[9] 6YZ5,[9] and 6ZXN[2]) were used for constructing the solvated H11-H4-RBD, H11-D4-RBD, and Ty1-RBD systems, respectively. Chloride ion, zinc ion, glycans, and water molecules present in the structures were kept. Full length glycans are not visible in the crystal structure. Thus, glycan models[33] were added to the structures. For conventional MD (cMD) simulations, each system was solvated in a water box (using the TIP3P water model) with a 25 Å cushion in each direction (50 Å water cushion between the protein complexes and their periodic images). For Steered MD[34] (SMD) simulations, systems were solvated having 50 Å cushion along the pulling direction in order to create enough space for unbinding simulations and 15 Å cushion in all other directions. Ions were added to neutralize the system and NaCl concentration was set to 150 mM. The size of solvated systems was ~150,000, ~120,000, and ~280,000 atoms for cMD, SMD, and RBD_{Delta}-PD-nanobody simulations, respectively. All system preparation steps were performed in VMD.

MD Simulation Details. All MD simulations were performed under N, P, T conditions in NAMD 2.14[35] using the CHARMM36[36] force field with a time step of 2 fs. Using the Langevin Nosé-Hoover method with an oscillation period of 100 fs and a damping time scale of 50 fs, the pressure was maintained at 1 atm. Using Langevin dynamics with a damping coefficient of 1 ps^{-1}, the temperature was kept at 310 K. For van der Waals interactions, 12 Å cutoff distance was used. To calculate long-range electrostatic interactions, Particle-mesh Ewald method was used. In all simulations periodic boundary conditions were applied. First, each system was minimized for 10,000 steps and subsequently equilibrated for 2 ns by keeping the protein fixed. A second minimization-equilibration cycle was performed: the complete system was minimized for additional 10,000 steps without fixing the protein, followed by 4 ns of equilibration by applying harmonic constraints on C_α atoms. As a final step before production runs, the constraints were released and the system was equilibrated for additional 4 ns. These simulations are expected to account for the structural differences due to the radically different thermodynamic conditions of

crystallization solutions and MD simulations.[37] MD simulations were performed in Longhorn, Expanse, and Stampede2 using a total of ~8.5 million core-hours.

Criteria for Interaction Analysis. Using MD simulation trajectories; salt bridges, hydrogen bonds, electrostatic and hydrophobic interactions were determined. For salt bridge formation, a cutoff distance of 6 Å between the basic nitrogen and acidic oxygen was used.[38] For hydrogen bond formation, a cutoff distance of 3.5 Å between hydrogen bond donor and acceptor, and a 30° angle between the hydrogen atom, the donor heavy atom and the acceptor heavy atom was used.[39] Interaction pairs that did not satisfy the angle criterion, but satisfied the distance criterion was classified as electrostatic interactions. For hydrophobic interactions, a cutoff distance of 8 Å between the side chain carbon atoms was used.[40-42] Observation frequencies were classified as high and moderate for interactions that occur in 49% and above and between 15 and 48% of the total trajectory, respectively.[28, 43] Pairwise interactions with observation frequencies below 15% were excluded from further analysis.

SMD Simulations. Steered and fixed atoms were selected as the C_α atoms at the nanobody-RBD and RBD-ACE2 interface (Table S1). The vector pointing from the center of mass of fixed atoms to the center of mass of steered atoms was selected as pulling direction (Figure S1). Each SMD simulation was performed until the rupture event is observed for each nanobody. Four different starting conformations for SMD simulations were taken from each MD simulations (conformations from 140, 160, 180, 200 ns).

RESULTS AND DISCUSSION

Interactions of Delta Variant RBD with ACE2. In our previous study, we determined the interaction network between RBD-PD by performing MD simulations of the RBD of WT SARS-CoV-2 S protein (RBD_{WT}) in complex with the PD of human ACE2.[28] To determine how RBD_{Delta} interacts with PD, we performed MD simulations of the RBD_{Delta}-PD complex. To obtain RBD_{Delta} structure, L452R and T478K mutations were manually introduced to the RBD_{WT} structure (PDB ID: 6M0J).[30] Two sets of cMD simulations, each of 200 ns in length (Table S2), were performed to determine the salt bridges,[38] hydrogen bonds, electrostatic and hydrophobic interactions (see Methods), and the results were compared to that of RBD_{WT} (Figure 2, Figure S3, and Table S3). We detected one new salt bridge (R403-E37), four new hydrophobic (A475-Y83, Y489-T27,

V503-T324, and Y505-F356) and five new electrostatic interactions at high frequencies in the RBD_{Delta}-PD complex compared to RBD_{WT} (Table 1). However, two high frequency hydrogen bond interactions (Q493-E35 and T500-D355) in RBD_{WT}-PD were observed in moderate frequencies in the RBD_{Delta}-PD complex (Table 1). In addition, we detected one new hydrogen bond (A475-S19), two new hydrophobic (Y421-T27 and V445-L45) and three new electrostatic interactions at moderate frequencies in the RBD_{Delta}-PD complex (Table S3). Three hydrogen bond interactions observed with moderate frequencies for RBD_{WT} (Y449-D38, Q498-Q42, and Q498-K353) were either observed at low frequencies or completely disappeared in RBD_{Delta}.

For RBD_{WT}, we divided the RBD-ACE2 interaction surface into three contact regions (CR1-3) and proposed that RBD-ACE2 interaction is primarily stabilized by hydrophobic interactions in CR1.[28, 44] Due to the Delta variant mutations, CR1 gains two hydrophobic interactions (A475-Y83 and Y489-T27) while CR2 remains unaffected. Remarkably, CR3 gains one salt bridge (R403-E37) and two hydrophobic interactions (V503-T324 and Y505-F356), while losing three hydrogen bonds (Y449-D38, Q498-Q42, and Q498-K343) with PD. In our previous study[28] we highlighted the role of CR1 in anchoring ACE2 and the importance in blocking its surface for S protein inhibition. Because CR3 also forms an extensive interaction network in the Delta variant, it may also be critical to target CR3 to prevent S-ACE2 interactions in the Delta variant.

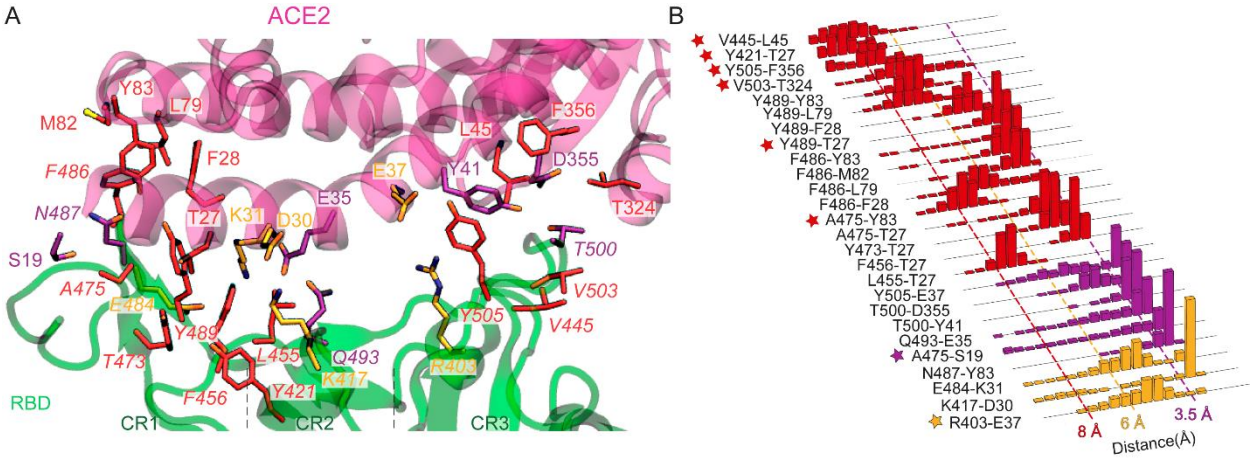

Figure 2. Interactions between SARS-CoV-2 S protein RBD and ACE2 PD. (A) Salt bridges, hydrogen bonds, and hydrophobic interactions between RBD_{Delta} and PD are shown in orange, purple, and red, respectively. RBD residue indices are shown in italic. Electrostatic interactions are listed in Table S3, (B) Normalized distributions of the distances between the amino-acid pairs that form salt bridges (orange), hydrogen bonds (purple), and hydrophobic interactions (red). The interactions newly observed for RBD_{Delta} with ACE2 are marked with stars.

Table 1. Net changes in the number of detected high frequency interactions between RBD and PD due to Delta variant mutations. Parentheses show (Number of interactions with RBD_{Delta}/Number of interactions with RBD_{WT})

	Salt Bridges	**Hydrogen Bonds**	**Hydrophobic Interactions**	**Electrostatic Interactions**
ACE2	+1 (3/2)	-2 (1/3)	+4 (15/11)	+4 (5/1)
H4	0 (1/1)	-2 (3/5)	-1 (9/10)	0 (1/1)
D4	0 (1/1)	-3 (2/5)	-2 (4/6)	+2 (2/0)
Ty1	0 (0/0)	-4 (1/5)	-4 (14/18)	+1 (1/0)

Interactions of RBD_{Delta} with H11-H4, H11-D4, and Ty1 Nanobodies. To investigate the interactions of the RBD_{Delta} with nanobodies, we introduced Delta variant mutations to the co-structure of SARS-CoV-2 S protein RBD in complex with H11-H4,[9] H11-D4,[9] and Ty1.[2] For each RBD_{Delta}-nanobody complex, two sets of cMD simulations, each of 200 ns in length (Table S1), were performed to determine pairwise interactions. Although H11-H4 and H11-D4 stayed bound to ACE2 in a binding mode throughout the simulations, Ty1 was observed to leave its original binding mode in one of the simulations (~100 ns into the simulation) and sampled various binding modes within 200 ns (Supplementary Movie S1). Thus, the interaction network for Ty1 is reported based on a single trajectory where it kept its original binding mode, while both trajectories are used for H11-H4 and H11-D4 (Figure 3, Figure S3, and Table S3).

Comparison of H11-H4's high frequency interactions with RBD_{WT} and RBD_{Delta}, shows that two hydrogen bonds (Y449-H100 and F490-Y104) and one hydrophobic interaction (L452-V102) were disappeared (Table 1). While L452-V102 disappeared completely, Y449-H100 and F490-Y104 were observed only with moderate frequencies for the Delta variant (Table S3). In addition, we detected one new hydrogen bond (Q493-Y101), two new hydrophobic (A475-Y104 and V483-A58) and three new electrostatic interactions at moderate frequencies (Table S3).

Similarly, for H11-D4, three of its hydrogen bonds (N450-E100, E484-S57, and S494-V102) and two of its hydrophobic interactions (L452-V102 and L455-L105) either completely disappeared (N450-E100, L452-V102 and L455-L105) or were observed at lower frequency (E484-S57 and S494-V102) with RBD_{Delta} (Table 1 and Figure S3). However, we detected two new electrostatic

interactions at high frequencies (Figure 3 and Table 1) and six new electrostatic interactions at moderate frequencies, while one electrostatic interaction observed with moderate frequency were only observed at low frequencies (Table S3).

For Ty1 nanobody, based on the single trajectory where binding to RBD_{Delta} was observed, three of its hydrogen bonds (E484-Y35, V483-V34, and S494-S107) and 11 of its hydrophobic interactions (L452-V102, I472-F29, I472-P55, I472-V34, L452-V4, L452-V109, L492-I100, L492-F29, F490-I100, F490-L6, and F490-L104) either completely disappeared or were observed at low frequency (Table 1 and Table S3). We detected seven new hydrophobic (Y351-V4, L455-L102, L455-L104, F456-L102, F456-L104, Y489-L102, and Y489-L104) and one new electrostatic interaction at high frequencies (Figure 3 and Table 1). Thus, the total number of hydrogen bonds and hydrophobic interactions observed at high frequency each decreased by four, while the total number of high frequency electrostatic interaction increased by one for the Delta variant (Table 1). In addition, we detected five new hydrogen bonds (S349-Q3, R452-R110, E484-L102, Q493-L102, and Q493-S107), one new hydrophobic (Y449-V109) and two new electrostatic interactions at moderate frequencies (Table S3). One hydrogen bond (E484-N56) and six electrostatic interactions observed with moderate frequencies completely disappeared. For the second set of Ty1-RBD_{Delta} MD simulation stable binding was not observed and all interactions observed in between Ty1 and RBD_{WT} completely disappeared.

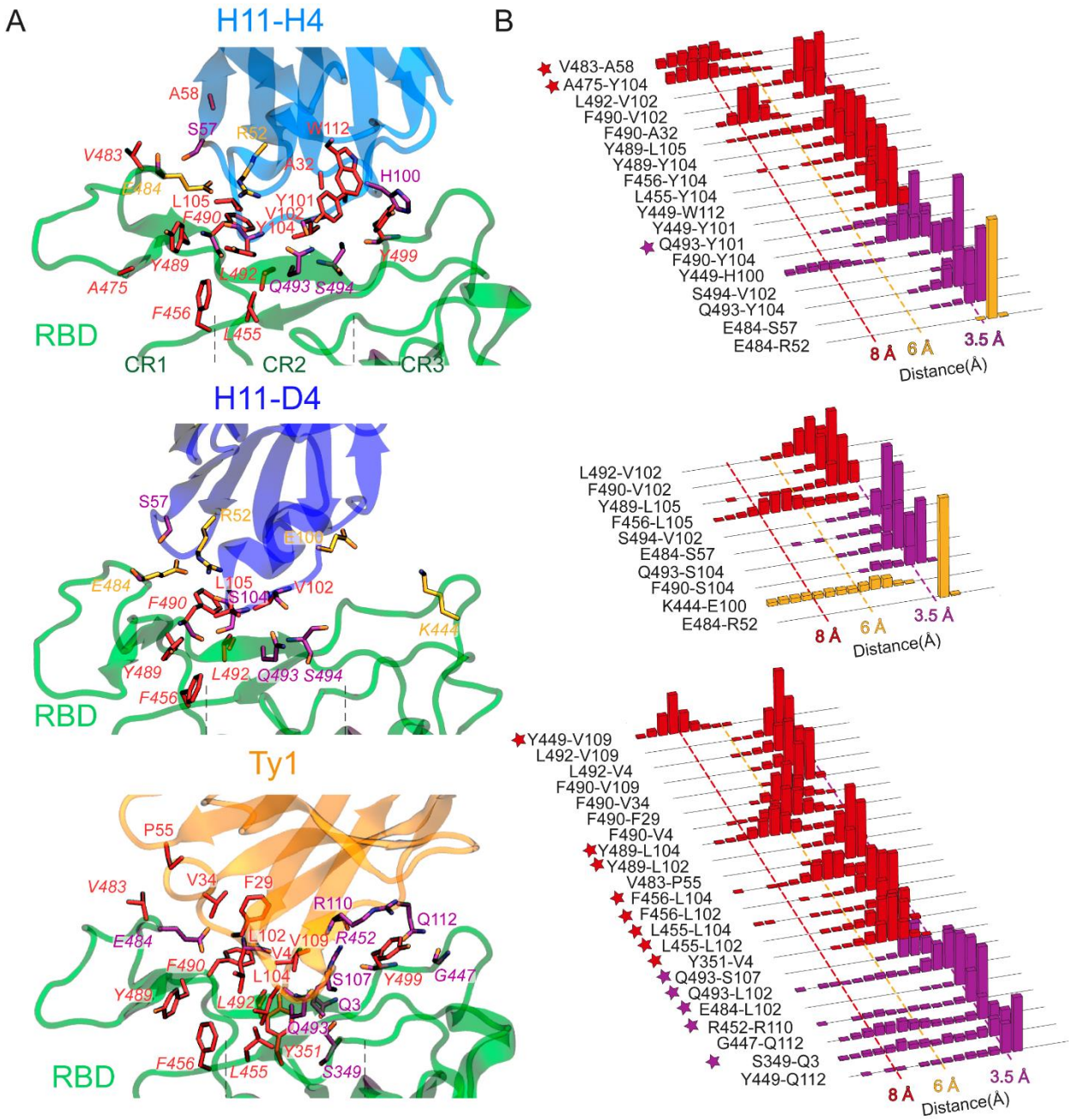

Figure 3. Interactions between SARS-CoV-2 S protein RBD and nanobodies. (A) Salt bridges (orange), hydrogen bonds (purple), and hydrophobic interactions (red) between RBD_{Delta} and nanobodies are shown. RBD residue indices are shown in italic. Electrostatic interactions are listed in Table S3, (B) Normalized distributions of the distances between the amino-acid pairs that form salt bridges, hydrogen bonds, and hydrophobic interactions are shown in orange, purple, and red, respectively. The interactions newly observed for RBD_{Delta} with nanobodies are marked with stars.

H11-H4 and H11-D4 Is Not Able to Abrogate ACE2 Binding to RBD_{Delta}. To investigate if H11-H4 or H11-D4 binding can disrupt RBD_{Delta}-PD interactions, we performed three sets of 200

ns cMD simulations of each RBD_{Delta}-PD-nanobody complex (Table S2). Nanobodies were manually docked onto the complex (PDB ID: 6M0J[30]) using the RBD-nanobody structure coordinates (PDB IDs: 6ZBP[9] and 6YZ5[9]). Although we previously showed that these nanobodies can dislocate PD from RBD_{WT} via the repulsion of identically charged residues,[43] they were unable to dislocate PD from RBD_{Delta} in any of our simulations (Figure 4). In contrast, H11-H4 was dislocated from its RBD binding pose in all three simulations (Supplementary Movie S2) due to the repulsion of identically charged residues of ACE2 and H11-H4 (ACE2 D67 with H11-H4 E44 and ACE2 K68 with H11-H4 R45, Figure 4) when ACE2 and H11-H4 are bound to RBD side-by-side. Therefore, while ACE2 loses the electrostatic tug-of-war against H11-H4 to bind RBD_{WT},[43] it outcompetes H11-H4 on RBD_{Delta} because of its increased and H11-H4's decreased interaction network with the RBD surface in the Delta variant.

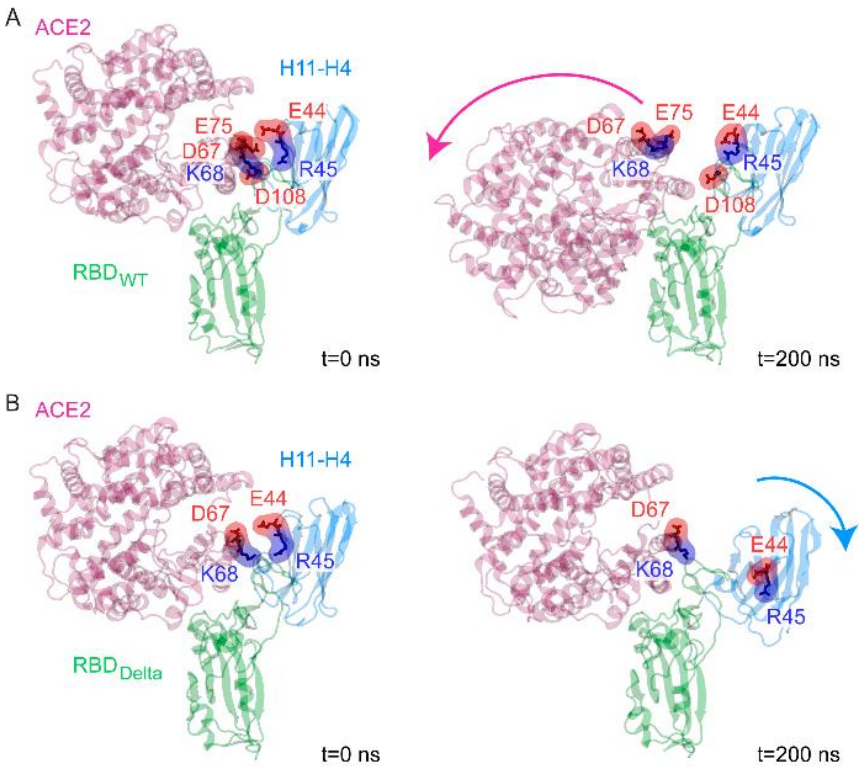

Figure 4. Effect of Delta variant RBD mutations onto the H11-H4's ability to dislocate ACE2. Electrostatic repulsion between ACE2 and H11-H4 upon H11-H4 docking on (A) RBD_{WT}[28, 43] and (B) RBD_{Delta}. Neighboring ACE2 and H11-H4 residues with identical charges are highlighted in surface representation in red (negatively charged) and blue (positively charged). H11-H4 binding resulted in 95% decrease in pairwise interaction observed between ACE2-RBD_{WT}, while H11-H4 it lost 54% of its interaction when bound to RBD_{Delta} with ACE2 side by side.

Similar to H11-H4, H11-D4 was neither able to dislocate ACE2 from RBD_{Delta} nor considerably affect its interaction with RBD_{Delta}. However, H11-D4 remained bound to RBD_{Delta} in the presence of PD, probably because it forms salt bridges R103-E35, R103-D38 and D108-K31 with ACE2 (Figure S3), while H11-H4 has serine at position 103 and is unable to form these salt bridges. Collectively, these results suggest substantially reduced nanobody effectiveness against the Delta variant.

Force-Induced Detachment of the Nanobodies from RBD. In order to estimate the binding strength of ACE2 and nanobodies to RBD_{Delta}, we performed SMD simulations at loading rates (a spring constant of 10 pN/Å and a pulling velocity of 0.1 Å/ns) comparable to those used in high-speed AFM experiments.[31] SMD simulations were performed by pulling the nanobodies at constant velocity along a vector pointing away from the binding interface (Figure S2). To be in accord with SMD studies on WT, Alpha and Beta variants,[43] RBD_{Delta} was pulled away from ACE2 to estimate ACE2's binding strength to RBD_{Delta}. Eight SMD simulations were performed for each system and their rupture forces were recorded (Figure 5 and Figure S4). Average rupture forces reduced by 5%, 19%, and 32% for H11-H4, H11-D4 and Ty1, respectively, when compared to ACE2. In our recent study, we had shown that for RBD_{WT}, H11-H4 has a higher binding strength while H11-D4 and Ty1 have a slightly lower binding strength than that of ACE2. Collectively, our in silico pulling experiments indicate that nanobodies are not able to bind stronger to the RBD_{Delta} compared to ACE2, and they also suggest that especially for H11-H4 there is a strong tendency for the binding strengths to decrease relative to ACE2.

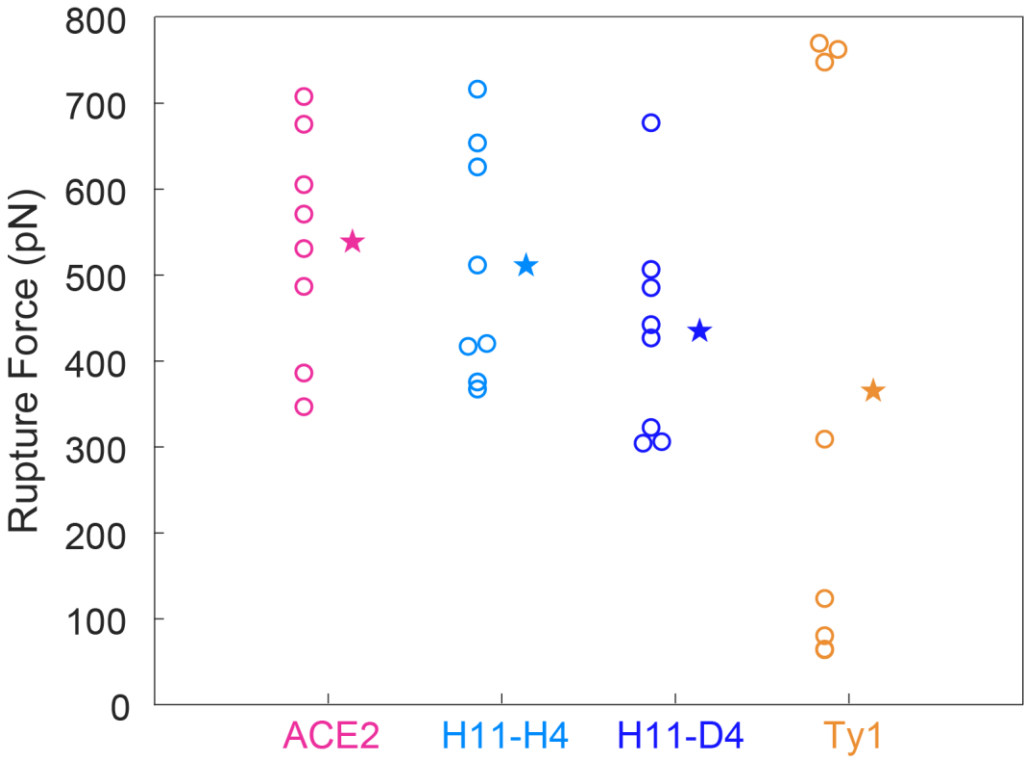

Figure 5. Ruptures forces recorded from in silico pulling experiments. Each rupture force recorded is provided with a circle while their averages are shown with stars.

CONCLUSIONS

In this study, we investigated how Delta variant mutations on the RBD of S protein affects its interactions with ACE2 and several nanobodies and determined whether these nanobodies are able to disrupt RBD_{Delta}-PD interactions by performing an extensive set of cMD simulations. To estimate rupture forces of the nanobodies and ACE2 from RBD_{Delta}, we also performed SMD simulations at loading rates (1 pN/ns) comparable to AFM studies, which are ~4-5 orders of magnitude lower than generally applied loading rates in SMD simulation. Thus, our SMD simulations provide a unique set of rupture forces that are directly comparable to experiments. Our simulations revealed that the Delta variant mutations lead to an increase in S protein-ACE2 interactions while decreasing the number of nanobody-S protein interactions. As a result, nanobodies H11-H4, H11-D4, and Ty1 have lower rupture forces from RBD_{Delta}. H11-H4 and H11-D4 remained stably bound to RBD_{Delta}, but they were unable to abrogate ACE2 binding when bound side by side on RBD_{Delta}. In comparison, Ty1 exhibited floppy binding in one of the two

simulations. Collectively, our results show the importance of identifying nanobodies for neutralizing specific variants of SARS-CoV-2[28, 43] and highlight the requirement of designing novel nanobodies to effectively neutralize the Delta variant.

In our previous study[28] we had shown that CR1 acts as the main anchor for SARS-CoV-2 S protein binding to ACE2, which is mainly facilitated through 10 hydrophobic interactions. Close inspection of the rupture events under load also showed that RBD_{WT} performs a zipper-like detachment with CR1 detaches the last in 80% of the simulations. In the Delta variant, CR1 forms two extra hydrophobic interactions, whereas CR3 gains one salt bridge and two hydrophobic interactions. CR1 detaches the last in five out of eight in silico pulling simulations whereas CR3 detaches either the last or at the same time with CR1 in other simulations. This difference may be attributed to an increase in the number of pairwise interactions in CR3. Therefore, it may be critical to target both CR1 and CR3 to effectively inhibit S-ACE2 interactions of the Delta variant.

Supporting Information

SMD simulation principles; Steered and fixed atoms in SMD simulations; The list of cMD and SMD simulations; Observation frequencies of interactions between RBD_{Delta} and PD and nanobodies; Pulling directions in SMD simulations; Electrostatic interactions of RBD_{Delta} with ACE2 PD and nanobodies; Salt bridges between ACE2 and H11-D4; Rupture forces from SMD simulations. (PDF)

Supplementary movie S1 shows the Ty1 leaving its original binding mode. (MP4)

Supplementary movie S2 shows the electrostatic repulsion between ACE2 and H11-H4 upon H11-H4 docking and H11-H4 dislocation for RBD_{Delta}. (MP4)

Data and Software Availability: All data and software are available upon request to the corresponding author.

Funding Sources

This work is supported by COVID-19 HPC Consortium (Grant number: TG-BIO200053).

Notes

The authors declare no competing financial interest.

ACKNOWLEDGMENT

This work used resources services, and support provided via the COVID-19 HPC Consortium (https://covid19-hpc-consortium.org/) and the Extreme Science and Engineering Discovery Environment (XSEDE), which is supported by National Science Foundation grant number ACI-1548562.

ABBREVIATIONS

μs, microsecond; ACE2, angiotensin-converting enzyme 2; AFM, atomic force microscopy; atm, standard atmosphere; Cα, alpha carbon; cMD, conventional molecular dynamics; CR, contact region; fs, femtosecond; MD, molecular dynamics; NAMD, nanoscale molecular dynamics; ns, nanosecond; NTD, n terminal domain; PD, peptidase domain; ps, picosecond; RBD, receptor-binding domain; mRNA, messenger ribonucleic acid; S, spike; SARS-CoV, severe acute respiratory syndrome-coronavirus; SMD, steered molecular dynamics; VMD, visual molecular dynamics; WT, wild type.

REFERENCES

1. Chakravarty, R.; Goel, S.; Cai, W., Nanobody: the "magic bullet" for molecular imaging? *Theranostics* **2014**, *4*, 386-398.
2. Hanke, L.; Vidakovics Perez, L.; Sheward, D. J.; Das, H.; Schulte, T.; Moliner-Morro, A.; Corcoran, M.; Achour, A.; Karlsson Hedestam, G. B.; Hällberg, B. M.; Murrell, B.; McInerney, G. M., An Alpaca Nanobody Neutralizes SARS-CoV-2 by Blocking Receptor Interaction. *Nat. Commun.* **2020**, *11*, 4420.
3. Wagner, T. R.; Ostertag, E.; Kaiser, P. D.; Gramlich, M.; Ruetalo, N.; Junker, D.; Haering, J.; Traenkle, B.; Becker, M.; Dulovic, A.; Schweizer, H.; Nueske, S.; Scholz, A.; Zeck, A.; Schenke-Layland, K.; Nelde, A.; Strengert, M.; Walz, J. S.; Zocher, G.; Stehle, T.; Schindler, M.; Schneiderhan-Marra, N.; Rothbauer, U., NeutrobodyPlex—monitoring SARS-CoV-2 neutralizing immune responses using nanobodies. *EMBO Rep.* **2021**, *22*, e52325.
4. Muyldermans, S., Nanobodies: Natural Single-Domain Antibodies. *Annu. Rev. Biochem* **2013**, *82*, 775-797.
5. Xu, J.; Xu, K.; Jung, S.; Conte, A.; Lieberman, J.; Muecksch, F.; Lorenzi, J. C. C.; Park, S.; Schmidt, F.; Wang, Z.; Huang, Y.; Luo, Y.; Nair, M. S.; Wang, P.; Schulz, J. E.; Tessarollo, L.; Bylund, T.; Chuang, G.-Y.; Olia, A. S.; Stephens, T.; Teng, I. T.; Tsybovsky, Y.; Zhou, T.; Munster, V.; Ho, D. D.; Hatziioannou, T.; Bieniasz, P. D.; Nussenzweig, M. C.; Kwong, P. D.; Casellas, R., Nanobodies from camelid mice and llamas neutralize SARS-CoV-2 variants. *Nature* **2021**, *595*, 278-282.
6. Raybould, M. I. J.; Kovaltsuk, A.; Marks, C.; Deane, C. M., CoV-AbDab: the coronavirus antibody database. *Bioinformatics* **2020**, *37*, 734-735.
7. Berman, H. M.; Westbrook, J.; Feng, Z.; Gilliland, G.; Bhat, T. N.; Weissig, H.; Shindyalov, I. N.; Bourne, P. E., The protein data bank. *Nucleic Acids Res.* **2000**, *28*, 235-242.
8. Wrapp, D.; De Vlieger, D.; Corbett, K. S.; Torres, G. M.; Wang, N.; Van Breedam, W.; Roose, K.; van Schie, L.; COVID, V.-C.; Team, R., Structural basis for potent neutralization of betacoronaviruses by single-domain camelid antibodies. *Cell* **2020**, *181*, 1004-1015. e15.
9. Huo, J.; Le Bas, A.; Ruza, R. R.; Duyvesteyn, H. M.; Mikolajek, H.; Malinauskas, T.; Tan, T. K.; Rijal, P.; Dumoux, M.; Ward, P. N., Neutralizing nanobodies bind SARS-CoV-2 spike RBD and block interaction with ACE2. *Nat. Struct. Mol. Biol.* **2020**, *27*, 846-854.
10. Zhou, D.; Duyvesteyn, H. M.; Chen, C.-P.; Huang, C.-G.; Chen, T.-H.; Shih, S.-R.; Lin, Y.-C.; Cheng, C.-Y.; Cheng, S.-H.; Huang, Y.-C., Structural basis for the neutralization of SARS-CoV-2 by an antibody from a convalescent patient. *Nat. Struct. Mol. Biol.* **2020**, *27*, 950-958.
11. Li, T.; Cai, H.; Yao, H.; Zhou, B.; Zhang, N.; van Vlissingen, M. F.; Kuiken, T.; Han, W.; GeurtsvanKessel, C. H.; Gong, Y., A synthetic nanobody targeting RBD protects hamsters from SARS-CoV-2 infection. *Nat. Commun.* **2021**, *12*, 1-13.
12. Xiang, Y.; Nambulli, S.; Xiao, Z.; Liu, H.; Sang, Z.; Duprex, W. P.; Schneidman-Duhovny, D.; Zhang, C.; Shi, Y., Versatile and multivalent nanobodies efficiently neutralize SARS-CoV-2. *Science* **2020**, *370*, 1479-1484.
13. Schoof, M.; Faust, B.; Saunders, R. A.; Sangwan, S.; Rezelj, V.; Hoppe, N.; Boone, M.; Billesbølle, C. B.; Puchades, C.; Azumaya, C. M., An ultrapotent synthetic nanobody neutralizes SARS-CoV-2 by stabilizing inactive Spike. *Science* **2020**, *370*, 1473-1479.

14. Ye, G.; Gallant, J.; Zheng, J.; Massey, C.; Shi, K.; Tai, W.; Odle, A.; Vickers, M.; Shang, J.; Wan, Y., The development of Nanosota-1 as anti-SARS-CoV-2 nanobody drug candidates. *Elife* **2021**, *10*, e64815.
15. Koenig, P.-A.; Das, H.; Liu, H.; Kümmerer, B. M.; Gohr, F. N.; Jenster, L.-M.; Schiffelers, L. D.; Tesfamariam, Y. M.; Uchima, M.; Wuerth, J. D., Structure-guided multivalent nanobodies block SARS-CoV-2 infection and suppress mutational escape. *Science* **2021**, *371*.
16. Pymm, P.; Adair, A.; Chan, L.-J.; Cooney, J. P.; Mordant, F. L.; Allison, C. C.; Lopez, E.; Haycroft, E. R.; O'Neill, M. T.; Tan, L. L., Nanobody cocktails potently neutralize SARS-CoV-2 D614G N501Y variant and protect mice. *Proceedings of the National Academy of Sciences* **2021**, *118*.
17. Baral, P.; Bhattarai, N.; Hossen, M. L.; Stebliankin, V.; Gerstman, B. S.; Narasimhan, G.; Chapagain, P. P., Mutation-induced changes in the receptor-binding interface of the SARS-CoV-2 Delta variant B.1.617.2 and implications for immune evasion. *Biochem. Biophys. Res. Commun.* **2021**, *574*, 14-19.
18. European Centre for Disease Prevention and Control. Emergence of SARS-CoV-2 B.1.617 variants in India and situation in the EU/EEA. ECDC: Stockholm. **May 11, 2021**.
19. Planas, D.; Veyer, D.; Baidaliuk, A.; Staropoli, I.; Guivel-Benhassine, F.; Rajah, M. M.; Planchais, C.; Porrot, F.; Robillard, N.; Puech, J.; Prot, M.; Gallais, F.; Gantner, P.; Velay, A.; Le Guen, J.; Kassis-Chikhani, N.; Edriss, D.; Belec, L.; Seve, A.; Courtellemont, L.; Péré, H.; Hocqueloux, L.; Fafi-Kremer, S.; Prazuck, T.; Mouquet, H.; Bruel, T.; Simon-Lorière, E.; Rey, F. A.; Schwartz, O., Reduced sensitivity of SARS-CoV-2 variant Delta to antibody neutralization. *Nature* **2021**, *596*, 276-280.
20. Lopez Bernal, J.; Andrews, N.; Gower, C.; Gallagher, E.; Simmons, R.; Thelwall, S.; Stowe, J.; Tessier, E.; Groves, N.; Dabrera, G.; Myers, R.; Campbell, C. N. J.; Amirthalingam, G.; Edmunds, M.; Zambon, M.; Brown, K. E.; Hopkins, S.; Chand, M.; Ramsay, M., Effectiveness of Covid-19 Vaccines against the B.1.617.2 (Delta) Variant. *N. Engl. J. Med.* **2021**, *385*, 585-594.
21. Liu, C.; Ginn, H. M.; Dejnirattisai, W.; Supasa, P.; Wang, B.; Tuekprakhon, A.; Nutalai, R.; Zhou, D.; Mentzer, A. J.; Zhao, Y.; Duyvesteyn, H. M. E.; López-Camacho, C.; Slon-Campos, J.; Walter, T. S.; Skelly, D.; Johnson, S. A.; Ritter, T. G.; Mason, C.; Costa Clemens, S. A.; Gomes Naveca, F.; Nascimento, V.; Nascimento, F.; Fernandes da Costa, C.; Resende, P. C.; Pauvolid-Correa, A.; Siqueira, M. M.; Dold, C.; Temperton, N.; Dong, T.; Pollard, A. J.; Knight, J. C.; Crook, D.; Lambe, T.; Clutterbuck, E.; Bibi, S.; Flaxman, A.; Bittaye, M.; Belij-Rammerstorfer, S.; Gilbert, S. C.; Malik, T.; Carroll, M. W.; Klenerman, P.; Barnes, E.; Dunachie, S. J.; Baillie, V.; Serafin, N.; Ditse, Z.; Da Silva, K.; Paterson, N. G.; Williams, M. A.; Hall, D. R.; Madhi, S.; Nunes, M. C.; Goulder, P.; Fry, E. E.; Mongkolsapaya, J.; Ren, J.; Stuart, D. I.; Screaton, G. R., Reduced neutralization of SARS-CoV-2 B.1.617 by vaccine and convalescent serum. *Cell* **2021**, *184*, 4220-4236.e13.
22. Schmitz, A. J.; Turner, J. S.; Liu, Z.; Zhou, J. Q.; Aziati, I. D.; Chen, R. E.; Joshi, A.; Bricker, T. L.; Darling, T. L.; Adelsberg, D. C.; Altomare, C. G.; Alsoussi, W. B.; Case, J. B.; VanBlargan, L. A.; Lei, T.; Thapa, M.; Amanat, F.; Jeevan, T.; Fabrizio, T.; O'Halloran, J. A.; Shi, P.-Y.; Presti, R. M.; Webby, R. J.; Krammer, F.; Whelan, S. P. J.; Bajic, G.; Diamond, M. S.; Boon, A. C. M.; Ellebedy, A. H., A vaccine-induced public antibody protects against SARS-CoV-2 and emerging variants. *Immunity* **2021**.

23. Wall, E. C.; Wu, M.; Harvey, R.; Kelly, G.; Warchal, S.; Sawyer, C.; Daniels, R.; Adams, L.; Hobson, P.; Hatipoglu, E., AZD1222-induced neutralising antibody activity against SARS-CoV-2 Delta VOC. *Lancet* **2021**, *398*, 207-209.
24. Corbett, K. S.; Werner, A. P.; Connell, S. O.; Gagne, M.; Lai, L.; Moliva, J. I.; Flynn, B.; Choi, A.; Koch, M.; Foulds, K. E.; Andrew, S. F.; Flebbe, D. R.; Lamb, E.; Nurmukhambetova, S. T.; Provost, S. J.; Bock, K. W.; Minai, M.; Nagata, B. M.; Ry, A. V.; Flinchbaugh, Z.; Johnston, T. S.; Mokhtari, E. B.; Mudvari, P.; Henry, A. R.; Laboune, F.; Chang, B.; Porto, M.; Wear, J.; Alvarado, G. S.; Boyoglu-Barnum, S.; Todd, J.-P. M.; Bart, B.; Cook, A.; Dodson, A.; Pessaint, L.; Steingrebe, K.; Elbashir, S.; Sriparna, M.; Pekosz, A.; Andersen, H.; Wu, K.; Edwards, D. K.; Kar, S.; Lewis, M. G.; Boritz, E.; Moore, I. N.; Carfi, A.; Suthar, M. S.; McDermott, A.; Roederer, M.; Nason, M. C.; Sullivan, N. J.; Douek, D. C.; Graham, B. S.; Seder, R. A., mRNA-1273 protects against SARS-CoV-2 beta infection in nonhuman primates. *Nat. Immunol.* **2021**.
25. Noori, M.; Nejadghaderi, S. A.; Arshi, S.; Carson-Chahhoud, K.; Ansarin, K.; Kolahi, A.-A.; Safiri, S., Potency of BNT162b2 and mRNA-1273 vaccine-induced neutralizing antibodies against severe acute respiratory syndrome-CoV-2 variants of concern: A systematic review of in vitro studies. *Rev. Med. Virol.* **2021**, e2277.
26. Gushchin, V. A.; Dolzhikova, I. V.; Shchetinin, A. M.; Odintsova, A. S.; Siniavin, A. E.; Nikiforova, M. A.; Pochtovyi, A. A.; Shidlovskaya, E. V.; Kuznetsova, N. A.; Burgasova, O. A.; Kolobukhina, L. V.; Iliukhina, A. A.; Kovyrshina, A. V.; Botikov, A. G.; Kuzina, A. V.; Grousova, D. M.; Tukhvatulin, A. I.; Shcheblyakov, D. V.; Zubkova, O. V.; Karpova, O. V.; Voronina, O. L.; Ryzhova, N. N.; Aksenova, E. I.; Kunda, M. S.; Lioznov, D. A.; Danilenko, D. M.; Komissarov, A. B.; Tkachuck, A. P.; Logunov, D. Y.; Gintsburg, A. L., Neutralizing Activity of Sera from Sputnik V-Vaccinated People against Variants of Concern (VOC: B.1.1.7, B.1.351, P.1, B.1.617.2, B.1.617.3) and Moscow Endemic SARS-CoV-2 Variants. *Vaccines* **2021**, *9*, 779.
27. Havervall, S.; Marking, U.; Greilert-Norin, N.; Ng, H.; Gordon, M.; Salomonsson, A. C.; Hellström, C.; Pin, E.; Blom, K.; Mangsbo, S.; Phillipson, M.; Klingström, J.; Hober, S.; Nilsson, P.; Åberg, M.; Thålin, C., Antibody responses after a single dose of ChAdOx1 nCoV-19 vaccine in healthcare workers previously infected with SARS-CoV-2. *EBioMedicine* **2021**, *70*, 103523.
28. Taka, E.; Yilmaz, S. Z.; Golcuk, M.; Kilinc, C.; Aktas, U.; Yildiz, A.; Gur, M., Critical Interactions Between the SARS-CoV-2 Spike Glycoprotein and the Human ACE2 Receptor. *J. Phys. Chem. B* **2021**, *125*, 5537-5548.
29. Kim, S.; Liu, Y.; Lei, Z.; Dicker, J.; Cao, Y.; Zhang, X. F.; Im, W., Differential Interactions Between Human ACE2 and Spike RBD of SARS-CoV-2 Variants of Concern. *J. Chem. Theory Comput.* **2021**, *17 (12)*, 7972-7979.
30. Lan, J.; Ge, J.; Yu, J.; Shan, S.; Zhou, H.; Fan, S.; Zhang, Q.; Shi, X.; Wang, Q.; Zhang, L., Structure of the SARS-CoV-2 Spike Receptor-Binding Domain Bound to the ACE2 Receptor. *Nature* **2020**, *581*, 215-220.
31. Rico, F.; Gonzalez, L.; Casuso, I.; Puig-Vidal, M.; Scheuring, S., High-Speed Force Spectroscopy Unfolds Titin at the Velocity of Molecular Dynamics Simulations. *Science* **2013**, *342*, 741-743.
32. Humphrey, W.; Dalke, A.; Schulten, K., VMD: Visual Molecular Dynamics. *J. Mol. Graph.* **1996**, *14*, 33-38.

33. Casalino, L.; Gaieb, Z.; Goldsmith, J. A.; Hjorth, C. K.; Dommer, A. C.; Harbison, A. M.; Fogarty, C. A.; Barros, E. P.; Taylor, B. C.; McLellan, J. S.; Fadda, E.; Amaro, R. E., Beyond Shielding: The Roles of Glycans in the SARS-CoV-2 Spike Protein. *ACS Cent. Sci.* **2020**, *6*, 1722-1734.
34. Isralewitz, B.; Gao, M.; Schulten, K., Steered Molecular Dynamics and Mechanical Functions of Proteins. *Curr. Opin. Struct. Biol.* **2001**, *11*, 224-230.
35. Phillips, J. C.; Hardy, D. J.; Maia, J. D.; Stone, J. E.; Ribeiro, J. V.; Bernardi, R. C.; Buch, R.; Fiorin, G.; Hénin, J.; Jiang, W., Scalable Molecular Dynamics on CPU and GPU Architectures with NAMD. *J. Chem. Phys.* **2020**, *153*, 044130.
36. Best, R. B.; Zhu, X.; Shim, J.; Lopes, P. E.; Mittal, J.; Feig, M.; MacKerell Jr, A. D., Optimization of the Additive CHARMM All-Atom Protein Force Field Targeting Improved Sampling of The Backbone ϕ, ψ and Side-Chain χ1 and χ2 Dihedral Angles. *J. Chem. Theory Comput.* **2012**, *8*, 3257-3273.
37. Pullara, F.; Wenzhi, M.; GÜR, M., Why Protein Conformers in Molecular Dynamics Simulations Differ from Their Crystal Structures: A Thermodynamic Insight. *Turk. J. Chem.* **2019**, *43*, 394-403.
38. Beckstein, O.; Denning, E. J.; Perilla, J. R.; Woolf, T. B., Zipping and unzipping of adenylate kinase: atomistic insights into the ensemble of open↔ closed transitions. *J. Mol. Biol.* **2009**, *394*, 160-176.
39. Durrant, J. D.; McCammon, J. A., HBonanza: a computer algorithm for molecular-dynamics-trajectory hydrogen-bond analysis. *J. Mol. Graph. Model.* **2011**, *31*, 5-9.
40. Stock, P.; Utzig, T.; Valtiner, M., Direct and Quantitative AFM Measurements of the Concentration and Temperature Dependence of the Hydrophobic Force Law at Nanoscopic Contacts. *J. Colloid Interface Sci.* **2015**, *446*, 244-251.
41. Manavalan, P.; Ponnuswamy, P., A Study of the Preferred Environment of Amino Acid Residues in Globular Proteins. *Arch. Biochem. Biophys.* **1977**, *184*, 476-487.
42. Stavrakoudis, A.; Tsoulos, I. G.; Shenkarev, Z. O.; Ovchinnikova, T. V., Molecular Dynamics Simulation of Antimicrobial Peptide Arenicin-2: b-Hairpin Stabilization by Noncovalent Interactions. *Biopolymers* **2009**, *92*, 143-155.
43. Golcuk, M.; Hacisuleyman, A.; Erman, B.; Yildiz, A.; Gur, M., Binding mechanism of neutralizing Nanobodies targeting SARS-CoV-2 Spike Glycoprotein. *J. Chem. Inf. Model.* **2021**, *61 (10)*, 5152-5160.
44. Wang, Y.; Liu, M.; Gao, J., Enhanced Receptor Binding of SARS-CoV-2 Through Networks of Hydrogen-Bonding and Hydrophobic Interactions. *PNAS* **2020**, *117*, 13967-13974.